Catalysis Today 166 (2011) 201–204

Contents lists available at ScienceDirect

Catalysis Today

journal homepage: www.elsevier.com/locate/cattod

Electro-reduction of nitrate species on Pt-based nanoparticles: Surface area effects

L.A. Estudillo-Wong[a], E.M. Arce-Estrada[b], N. Alonso-Vante[c], A. Manzo-Robledo[a,*]

[a] Laboratorio de Electroquímica y Corrosión, Escuela Superior de Ingeniería Química e Industrias Extractivas (ESIQIE)-IPN, México D.F., Mexico
[b] Departamento de Ingeniería Metalúrgica. Escuela Superior de Ingeniería Química e Industrias Extractivas (ESIQIE)-IPN, México D.F., Mexico
[c] Laboratoire d'Electrocatalyse, UMR-CNRS 6503, Université de Poitiers, F-86022 Poitiers, France

ARTICLE INFO

Article history:
Available online 14 October 2010

Keywords:
Nitrate reduction
Hydrogen evolution reaction
Nanoparticles
Cyclic voltammetry
Electrocatalysis

ABSTRACT

The electrochemical reduction of nitrate ions was carried out on Pt-based nanoparticles supported on carbon Vulcan and deposited on a glassy carbon electrode. Different materials were evaluated: synthesized Pt_{10}/C, Pt–Sn_y/C (y = 10, 20 wt.%) and commercial Pt_x/C-ETEK (x = 10, 20 and 40 wt.%). Cyclic voltammetry technique was used for this purpose. It was found that the catalytic activity for hydrogen evolution reaction (HER) and nitrate electro-reduction (NER) follows the order Pt_{10}/C > Pt_{40}/C-ETEK > Pt–Sn_{20}/C > Pt_{20}/C-ETEK > Pt–Sn_{10}/C > Pt_{10}/C-ETEK. The electrochemically active surface area (ECSA), charge due to nitrate electro-reduction ($Q_{NO_3^-}$), and kinetic parameters were calculated in order to understand the catalytic behavior.

1. Introduction

Pollution control of water sources, soil and air has motivated the interest in nanotechnology [1–3] as well as the implement of new techniques [4–10]. The increasing demand of materials to be used in normal conditions has led to the development of catalysts with small particles size well dispersed in the support matrix (e.g. carbon Vulcan). These properties modify and might enhance the catalytic effect at the electrode–electrolyte interface. For this purpose, the preparation route should be considered. Carbonyl chemical route (CCR) allows obtaining materials in the nanolength scale (e.g. 1–3 nm). Initial studies with platinum-based materials and other metals were carried out by Longoni and Chini [11] followed by Johnson, Lewis and recently by Alonso-Vante [12].

It is well known that pollution of water sources with nitrates is a challenge for environmental sciences [13–18]. In non-developed countries, 20% of NO_x emissions (source of nitrate ions) are neither controlled nor eliminated [19]. Numerous techniques have been proposed for their elimination; however, these techniques present, in general, high costs [13,18]. On the other hand, nitrate electro-reduction (NER) has been extensively studied in recent years [18,20–22]. NER reaction is a multi-electron transfer process showing different mechanisms as a function of pH, nitrate and supporting electrolyte concentration, particle size-distribution as well as electrochemically active surface area (ECSA) of the catalyst [20–23].

In this study, Pt-based nanoparticles prepared by carbonyl route, Pt/C (10 wt.% Pt), Pt–Sn_y/C (y = 10 and 20 wt.%), were evaluated and their electrochemical performance was compared with Pt from commercial source. Cyclic voltammetry technique was used in alkaline conditions and different nitrate concentrations.

2. Experimental

Mono- and bi-metallic nanoparticles were prepared as previously described [11,12,24]. Commercial source was from ETEK: 10, 20 and 40 wt.% Pt/C. Four milligrams of catalysts synthesized or commercial, 4 μL of Nafion solution (5 wt.%, Aldrich) and 1 mL of water were mixed ultrasonically. 4 μL of this ink was transferred via a syringe onto a freshly polished glassy carbon (GC) disk (4 mm of diameter) and then dried in atmosphere of argon for 30 min. Electrochemical measurements were performed using an EG&G potentiostat/galvanostat (model 263A) and a conventional three-electrode electrochemical cell. The counter electrode was a glassy carbon plate and a standard calomel electrode (SCE) served as a reference electrode. This latter was connected to the working electrode compartment by a Luggin capillary. Prior to any measurements, the working electrode was cycled until reproducible $i-E$ characteristics of platinum were obtained in a 0.5 M H_2SO_4 solution at scan rate of 50 mV s^{-1}. The nitrate concentration was varied from 0.001 to 1.0 M in NaOH 0.5 M as supporting electrolyte at 5 mV s^{-1}. High purity argon was used to purge of the solution.

* Corresponding author. Tel.: +52 5557296000; fax: +52 5555862728.
E-mail address: amanzor@ipn.mx (A. Manzo-Robledo).

0920-5861/$ – see front matter © 2010 Elsevier B.V. All rights reserved.
doi:10.1016/j.cattod.2010.09.010

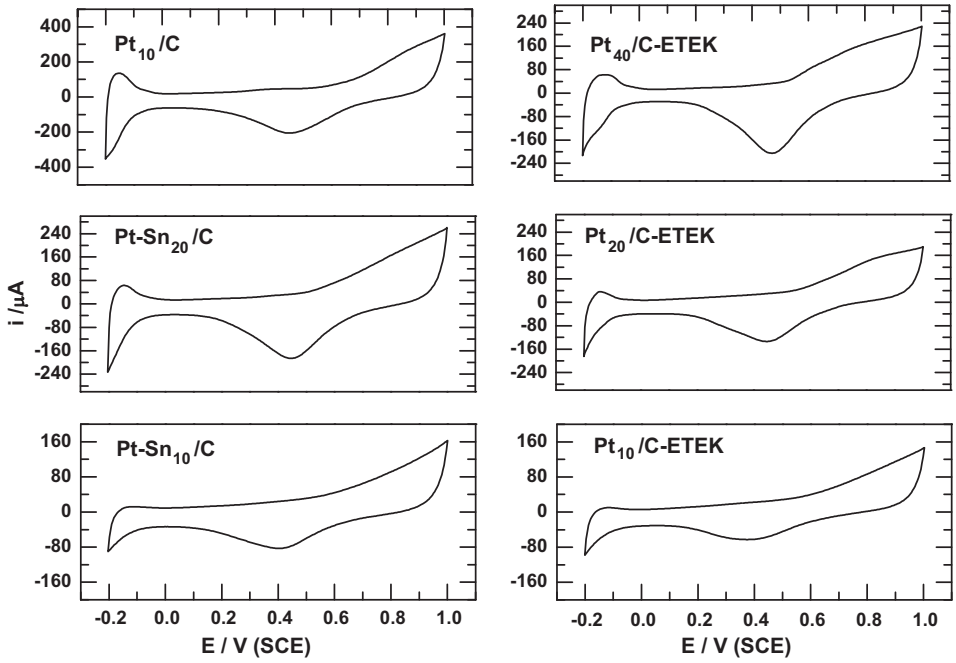

Fig. 1. $i-E$ characteristics for Pt-based nanoparticles in 0.5 M H_2SO_4. $v = 50\,mV\,s^{-1}$.

During the measurements, a gentle flow of this gas was maintained above the electrolyte surface. The electrochemical measurements were performed at room temperature. All chemicals used were of analytical grade and the solutions were prepared with ultra-pure water.

3. Results and discussion

3.1. Electrochemical characterization

The Pt-based nanoparticles were characterized and activated in a potential window from −0.2 to 1 V/SCE. Fig. 1 depicts the $i-E$ profiles in 0.5 M H_2SO_4 solution at scan rate of 50 mV s^{-1}. As can be seen from this figure, Pt_{10}/C presents more intense surface redox waves than 20 wt.%, and 40 wt.% Pt/C-ETEK, and the bimetallic 20 wt.% Pt–Sn/C. In order to compare the performance of these materials, the electrochemically active surface area (ECSA) was calculated in the hydrogen adsorption–desorption zone (Q_H) according to Eq. (1):

$$Q_H = \frac{1}{\nu}\int_{E_i}^{E_f} i(E)dE - Q_{dl} \quad (1)$$

where E_i and E_f are the initial and final potentials corresponding to underpotential deposition of hydrogen (H_{upd}) from 0.038 to −0.2 V/SCE, respectively; and (Q_{dl}) is the double layer charge. The ECSA (Sr_{Pt}), using Eq. (2) can be obtained with $Q_{Pt} = 210\,\mu C\,cm^{-2}$ [18,25]:

$$S_r = \frac{Q_H}{Q_{Pt}} \quad (2)$$

The results obtained from Eqs. (1) and (2) are summarized in Table 1. One observes that ECSA decreases in the order Pt_{10}/C > Pt_{40}/C-ETEK > Pt–Sn_{20}/C > Pt_{20}/C-ETEK > Pt–Sn_{10}/C > Pt_{10}/C-ETEK.

3.2. Electrochemical reduction of nitrate species

In order to compare the electrocatalytic activities for NER, Fig. 2 shows the $i-E$ profiles for different $NaNO_3$ concentration (1, 0.1, 0.01, 0.001 M) on (a) Pt_{10}/C-ETEK, (b) Pt_{20}/C-ETEK and (c) Pt_{40}/C-ETEK electrodes. The scan rate was fixed at 5 mV s^{-1} from 0.2 to −1.0 V/SCE. For all the three samples, the redox phenomena attributed to electrochemical reduction of nitrate ions are evident in the potential interval from ca. −0.6 to −0.9 V/SCE. These redox profiles are similar to those obtained for synthesized Pt_{10}/C, inset in Fig. 2a; see Ref. [22] for more details. Furthermore, the reduction current peak (i_p) increases as a function of nitrate concentration. At the positive going scan, the peak labeled (i_a) can be attributed to oxidation processes of the nitrate reduction in the negative going scan. Also, the magnitude of i_a decreases as NO_3^- concentration decreases. The current intensity at (i_p) and (i_a) becomes higher as a function of Pt loading. Similar profiles were found on bimetallic nanoparticles, see Fig. 3. According to this, three processes are associated to the profiles depicted in Figs. 2 and 3, namely (i) nitrate electro-reduction (i_p), (ii) hydrogen evolution reaction (HER), at potential more negative than −0.9 V/SCE, induced by proton adsorption [26], and (iii) oxidation of reduced species at the negative going scan (i_a) [22]. It is important to note that at concentrations lower than 0.01 M of nitrates, only the HER takes place (solid lines, Figs. 2 and 3).

The reaction order (β) and reaction rate constant (k_f) were calculated using the profiles depicted in Figs. 2 and 3 with respect to nitrate concentration [27] in a potential region where pure kinetic phenomena are carried out ($E = -0.78$ V/SCE), Eq. (3).

$$\log i_E = \log k_f + \beta \log[NO_3^-] \quad (3)$$

The average value of β, obtained from the profiles depicted in Fig. 4, was 0.26 ± 0.08, see Table 2. In some way, this value put in evidence the inherent complexity of the interactions of NO_3^- with

Table 1
Adsorption–desorption charge (Q_H) and ECSA (Sr_{Pt}) for Pt-based catalysts.

Catalyst	Q_H (μC)	[a] Sr_{Pt} (cm^2)
Pt_{10}/C	547.8	3.0
Pt_{40}/C-ETEK	327.5	1.8
Pt–Sn_{20}/C	285.3	1.6
Pt_{20}/C-ETEK	171.1	0.9
Pt_{10}/C-ETEK	78.6	0.4
Pt–Sn_{10}/C	60.3	0.3

[a] Calculated with $Q_{Pt} = 210\,\mu C\,cm^{-2}$.

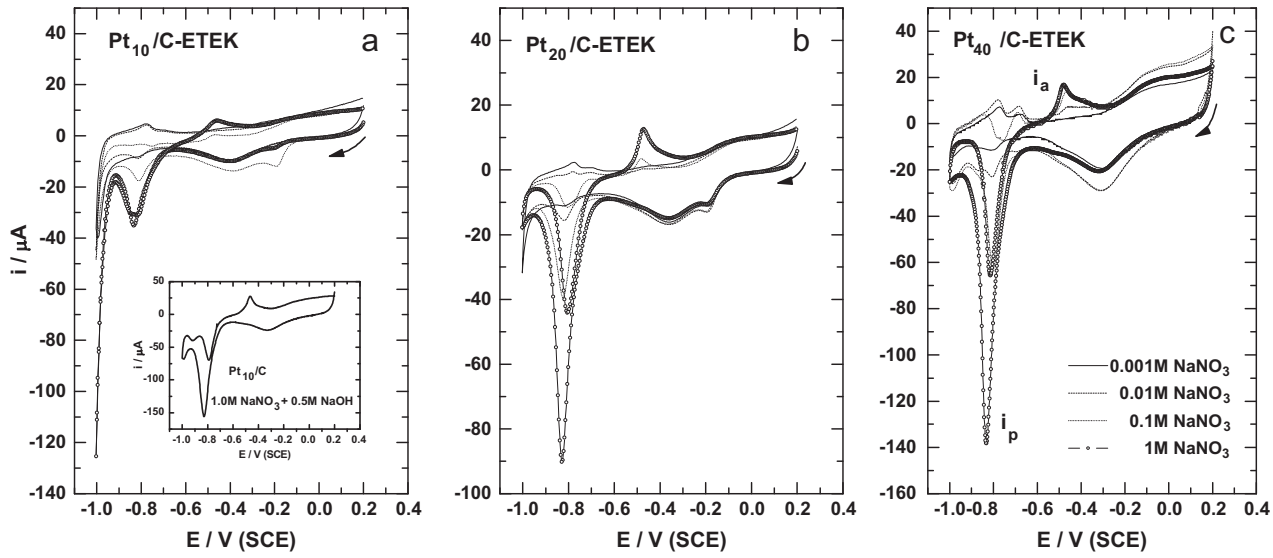

Fig. 2. $i-E$ characteristics for Pt/C-ETEK at different nitrate concentration. Inset: characteristic of synthesized Pt_{10}/C. $v = 5\,mV\,s^{-1}$.

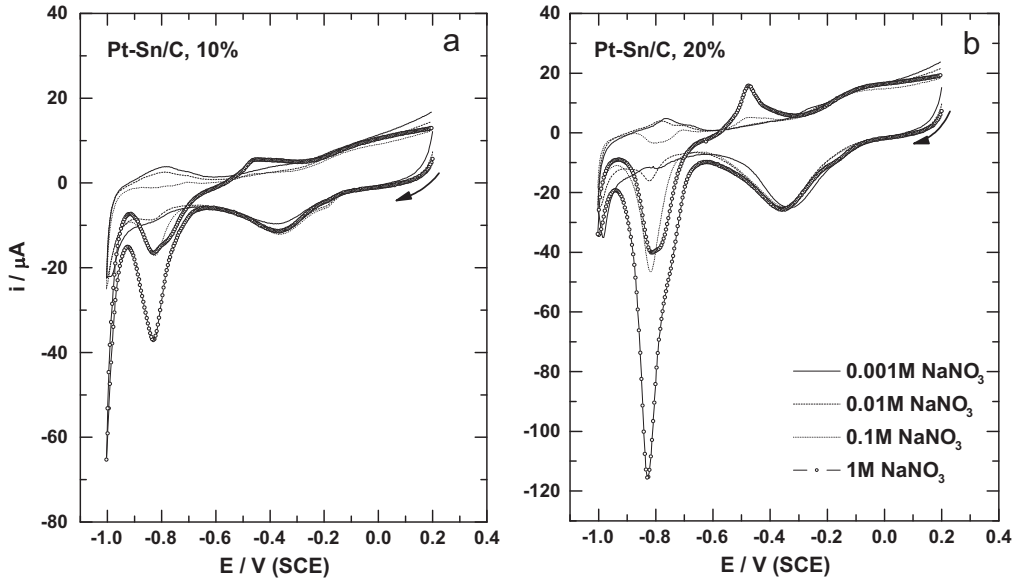

Fig. 3. $i-E$ characteristic for Pt–Sn/C nanoparticles at different nitrate concentration. $v = 5\,mV\,s^{-1}$.

protons (see region I_a and II_a in Fig. 5) that occur at the catalytic available active surface sites ($\theta_{NO_3^-}/1-\theta_{NO_3^-}$) [28], as a function of pH and supporting electrolyte concentration, Fig. 5. In this context, adsorbed intermediates (protons and/or reaction products) might compete and/or block the catalytic sites for (subsequent) nitrate-ion adsorption as a function of initial $\theta_{NO_3^-}$. For example, the nitrate reduction charge (from inset in Fig. 2) was 3100 μC after proton adsorption-charge correction from curve (a) in Fig. 5 ($Q_H = 980\,\mu C$) in the interval from −0.6 to −0.93 V/SCE. In addition, depending on local pH, molecular nitrogen or NH_2OH could be formed at the electrode interface [29]. On the other hand, taking into account the value of k_f from Table 2, the catalytic activity versus NER followed the order $Pt_{10}/C > Pt_{40}/C\text{-ETEK} > Pt\text{–}Sn_{20}/C > Pt_{20}/C\text{-ETEK} > Pt\text{–}Sn_{10}/C > Pt_{10}/C\text{-ETEK}$; in agreement with the ECSA calculated in acid conditions, see Table 1. Therefore, the evidences shown here, indicate that the nitrate electro-reduction is controlled by proton adsorption and ECSA. Such assumptions explain the better performance of the homemade electrocatalyst.

In order to establish a link between the catalytic activity of these nanomaterials versus NER and ECSA, the charge of nitrate ($\theta_{NO_3^-}$) was evaluated in a potential window from −0.9 to −0.6 V/SCE, using

Table 2
Reaction order (β) and reaction rate constant (k_f) for Pt-based nano-materials.

Catalyst	β[a]	$k_f\,\mu A\,(mol\,L^{-1})a^{-\beta}$
Pt_{10}/C	0.27	94.65
Pt_{40}/C-ETEK	0.25	65.81
$Pt\text{–}Sn_{20}/C$	0.39	64.16
Pt_{20}/C-ETEK	0.29	41.39
Pt_{10}/C-ETEK	0.24	21.06
$Pt\text{–}Sn_{10}/C$	0.14	19.91

[a] Calculated at $E = -780$ mV/SCE.

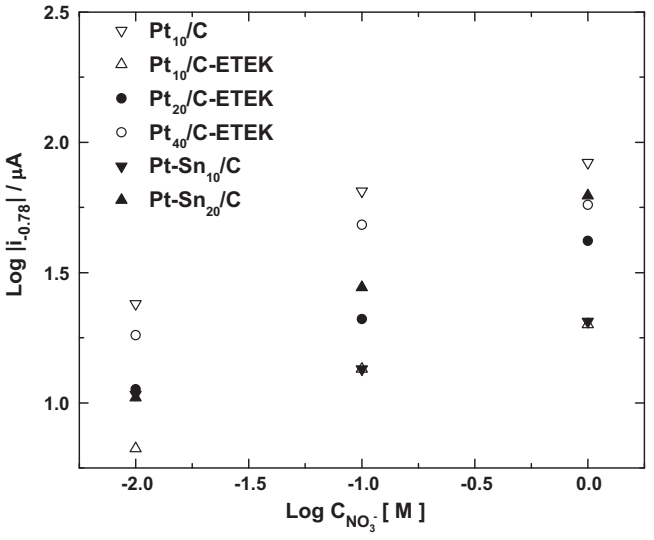

Fig. 4. Log $|i_{-0.78}|$ versus log $C_{NO_3^-}$ for Pt-based nanoparticles.

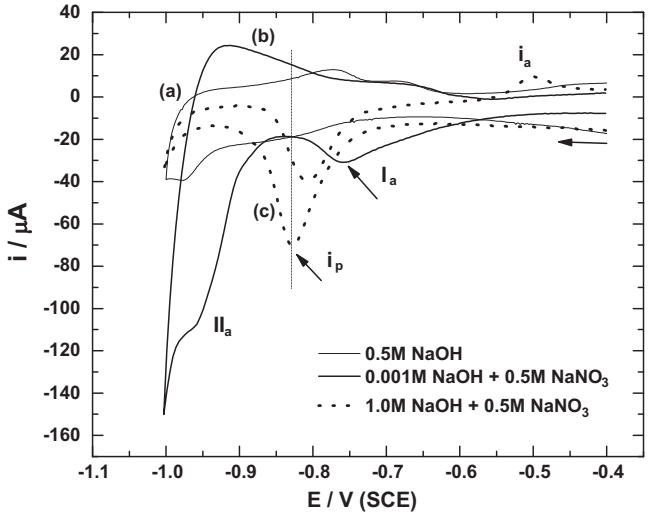

Fig. 5. $i-E$ characteristics for Pt_{10}/C in a solution of 0.0001 M + 0.5 M $NaNO_3$ (b) and 1.0 M NaOH + 0.5 M $NaNO_3$ (c). Curve (a) is the characteristic obtained at the supporting electrolyte (0.5 M NaOH) free of nitrates. Scan rate of 5 mV s^{-1}.

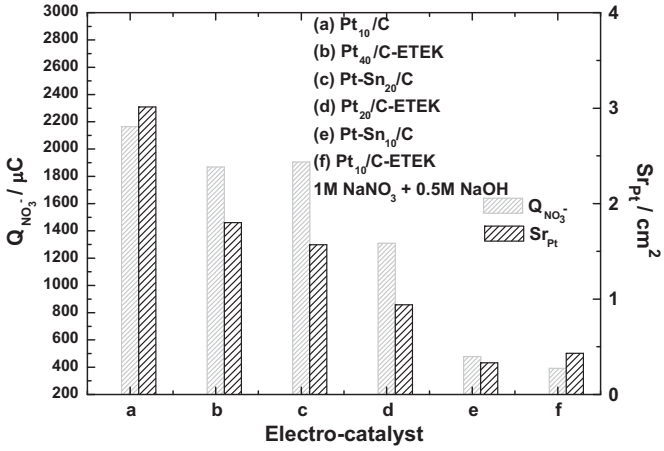

Fig. 6. Nitrate electro-reduction charge (μC) and active surface for Pt-based nanoparticles.

Eq. (1). The results are depicted in Fig. 6. It is clear that an intrinsic relationship between the charge of nitrate reduction and the active surface area exist. For instance, pure electrochemical calculations (Q_H, $\theta_{NO_3^-}$ and ECSA) permit the evaluation of critical nanomaterials properties such as catalytic activity. Indeed, these parameters provide indirect information about the state of the nanoparticles in the support matrix.

4. Conclusions

The electrochemical reduction of nitrates was accomplished using monometallic and bimetallic nanostructures based on platinum. Pt_{10}/C prepared via carbonyl chemical route (CCR) presents the best performance toward HER and NER reactions, followed by Pt_{40}/C-ETEK and Pt–Sn_{20}/C (also synthesized via CCR). Therefore, adding a second metal confers an electrochemical activity similar to that of Pt_{40}/C-ETEK. The lower catalytic performance was presented at Pt_{20}/C-ETEK, Pt–Sn_{10}/C and Pt_{10}/C-ETEK. In this context, the difference in the catalytic activity versus NER between Pt_{10}/C and its commercial counterpart (Pt_{10}/C-ETEK) is about 80%, indicating that the preparation route has an important impact for activity. Indeed, the electrochemical parameter calculated (Q_H, $\theta_{NO_3^-}$ and ECSA) can be an important tool to elucidate critical nanomaterials properties.

Acknowledgments

The authors thank the financial support giving through the project ESIQIE-IPN-CGPI 20090921, 20090501, 20100136 and ICyTDF-PICS08-29, as well as COFAA and SNI-CONACyT.

References

[1] B. Nordell, Global Planet. Change 38 (2003) 305.
[2] M. Gavrilescu, L.V. Pavel, I. Cretescu, J. Hazard. Mater. 163 (2009) 475.
[3] A.G. Mamalis, J. Mater. Process. Technol. 181 (2007) 52.
[4] I. Cretescu, J. Hazard. Mater. 163 (2009) 475.
[5] S. Hörold, K.-D. Vorlop, T. Tacke, M. Sell, Catal. Today 17 (1993) 21.
[6] T. Filofteia-Laura, G. Bertrand, S. Ok Chwa, C. Meunier, D. Klein, C. Coddet, Surf. Coatings Technol. 200 (2006) 5855.
[7] J.J. Schoeman, A. Steyn, Desalination 255 (2003) 25.
[8] S.G. Lehman, M. Badruzzaman, S. Adham, D.J. Roberts, D.A. Clifford, Water Res. 42 (2008) 969.
[9] T. Lie, J. Farrell, Environ. Sci. Technol. 35 (2001) 3560.
[10] H.C. Yang, Y.J. Cho, H.C. Heun, E.H. Kim, Chem. Eng. Sci. 62 (2007) 5137.
[11] G. Longoni, P. Chini, J. Am. Chem. Soc. 98 (1976) 7225.
[12] N. Alonso-Vante, Fuel Cells 3 (2006) 182.
[13] J.M. Rodríguez-Maroto, F. García-Herruzo, A. García-Rubio, C. Gómez-Lahoz, C. Vereda-Alonso, Chemosphere 74 (2009) 804.
[14] K. Jha, J.W. Weidner, J. Appl. Electrochem. 29 (1999) 1305.
[15] I. Katsounaros, G. Kyriacou, Electrochim. Acta 53 (2008) 5477.
[16] D. Reyter, D. Bélanger, L. Roue, Electrochim. Acta 53 (2008) 5977.
[17] B. Sang-Eun, K.L. Stewart, A.A. Gewirth, J. Am. Chem. Soc. 129 (2007) 10171.
[18] L.A. Estudillo-Wong, Bachelor thesis, ESIQIE-IPN, México, 2008.
[19] M.T. Lopéz, M. Zuck, V. Garibay, G. Tzintzun, R. Iniestra, A. Fernández, Atmos. Environ. 39 (2005) 1199.
[20] A. Manzo-Robledo, C. Levy-Clement, N. Alonso-Vante, Langmuir 23 (2007) 11413.
[21] A. Manzo-Robledo, Ph.D. thesis, Poitiers University, France, 2004.
[22] L.A. Estudillo Wong, N. Alonso Vante, A. Manzo Robledo, ECS Trans. 25 (2008) 385.
[23] O. Brylev, M. Sarrazin, D. Bélanger, L. Roué, Electrochim. Acta 52 (2007) 6237.
[24] A. Manzo-Robledo, A.-C. Boucher, E. Pastor, N. Alonso-Vante, Fuel Cells 2 (2002) 2.
[25] B. Lim, M. Jiang, P.H.C. Camargo, E.C. Cho, J. Tao, X. Lu, Y. Zhu, Y. Xia, Science 324 (2009) 1302.
[26] S. Taguchi, J.M. Feliu, Electrochim. Acta 53 (2008) 3626.
[27] D. Reyter, G. Chamoulaud, D. Bélanger, L. Roué, J. Electroanal. Chem. 596 (2006) 13.
[28] B.E. Conway, H.A. Kozlowska, H.P. Dhar, Electrochim. Acta 19 (1974) 455.
[29] G.E. Badea, Electrochim. Acta 54 (2009) 996.